



Effect of cannelure fin configuration on compact aircooling heat sink

Chi-Chuan Wang^{a,*}, Kai-Shing Yang^b, Yang-Ping Liu^c, Ing Youn Chen^c

^aDepartment of Mechanical Engineering, National Chiao Tung University, EE474, 1001 University Road, Hsinchu 300, Taiwan

^bGreen Energy & Environment Laboratories, Industrial Technology Research Institute, Hsinchu 310, Taiwan

^cMechanical Engineering Department, National Yunlin University of Science and Technology, Yunlin 640, Taiwan

ARTICLE INFO

Article history:

Received 8 September 2010

Accepted 1 February 2011

Available online 12 February 2011

Keywords:

Heat sink

Interrupted fin

Dimple/cavity vortex generator

Cannelure

ABSTRACT

The present study proposed a novel cannelure fin structure applicable to compact air-cooled heat sink under cross flow condition. A total of eight heat sinks were made and tested, including plain fin, oblique dimple type (I), oblique dimple type (II), straight cannelure, full oblique cannelure, half oblique cannelure with dimple/cavity type, half oblique cannelure with dimple/cavity type (II), and full oblique cannelure with dimple/cavity. Test results indicate that the proposed full cannelure fin along with the dimple/cavity structure can attain approximately 25% increase of heat transfer performance, and accompanies a friction reduction of about 20%. Moreover, converse to those interrupted fin or triangular vortex generator, it is found that the proposed fin structure still offers significant augmentation in fully developed region. The observed IR image of the temperature measurement of the test fin configurations also confirms the measurements.

© 2011 Elsevier Ltd. All rights reserved.

1. Introduction

High power electronics are testing the limits of traditional cooling methods. Effective heat removal is required to keep silicon junction temperatures below critical temperatures at which devices will fail. Although liquid cooling with or without phase change are often regarded as the major candidates for high flux applications, air cooling is still by far the most common cooling technique for electronic cooling for its simplicity, reliability, and low cost.

However, an interminable rise of concentrated heat source seems to place barricades for direct air-cooling and one must look for other indirect alternatives like liquid cooling, refrigeration, thermoelectric, loop heat pipe, vapor chamber, nucleate boiling, spray cooling, and other possible heat spreading devices such as micro-channel heat exchangers [1]. For direct air-cooling, Saini and Webb [2] found a practical limit of thermal resistance, suggesting a value of 0.221 K/W which will give 89.4 W heat rejection for impinging flow, as compared to 75.1 W for duct flow.

Theoretically, the air-cooled heat sink can accommodate more fin surface to reduce thermal resistance by reducing the fin spacing. However, it will result in a dramatic pressure drop along with fully developed flow leading to a deterioration of heat transfer performance. Hence, instead of adding fin surfaces, exploiting enhanced surface is often regarded as an effective to promote heat transfer for compact heat sink.

One of the first ideas to enhance air-cooled heat sink is via interrupted surface. It is reported by Yang et al. [3] who employed the interrupted surfaces such as louver or slit fin in their compact heat sink, and they reported that the interrupted surfaces can effectively restart the boundary layer to achieve a higher heat transfer performance provided the fin spacing is not too small (normally $F_s > 1.6$ mm). Nevertheless the interrupted surfaces also accompany appreciable pressure drop penalty. On the other hand, Yang et al. [3] also found a significant drop of heat transfer performance at the low Reynolds number at a very small fin spacing ($F_s = 0.8$ mm). This is because fully developed flow prevails. Note that the general concept for interrupted surface is via periodical renewal of boundary layer. Unfortunately, as pointed out by Yang et al. [3] and Webb and Trauger [4], typical interrupted surfaces like louver fin shows appreciable degradation in low velocity region pertaining to the “duct flow” phenomenon. The appreciable level-off of the heat transfer coefficient at this low velocity region for the louver fin geometry had been reported by some investigators. For example, Davenport [5] and Achaichia and Cowell [6] had reported that the deterioration of heat transfer coefficients in the low velocities region from their test results of an automotive multi-louver fin surface. Webb and Trauger [4] found that at a low Reynolds number some of the air streams bypass the louvers and act as “duct flow” between the fin channels, giving rise to a lower j factor. Unfortunately, most electronic cooling applications fall into this category, thereby implicating the inability of interrupted surfaces for very compact heat sink.

* Corresponding author.

E-mail address: [ccwang@itri.org.tw](mailto:cwang@itri.org.tw) (C.-C. Wang).

Nomenclature

A	heat transfer surface area (m ²)
A_{ct}	minimum flow area, based on one flow channel (m ²)
A_{front}	Frontal area of the test section (m ²)
$A_{ft,hs}$	cross sectional area of fins (m ²)
Cp_a	specific heat at constant pressure of air (J/kg K)
d	dimple print diameter (m), shown in Table 1
D	dimple diameter (m), shown in Table 1
D_h	hydraulic diameter (m)
f	friction factor (dimensionless)
F_s	fin spacing (m)
\bar{h}	average convective heat transfer coefficient (W/m ² K)
j	Colburn factor (dimensionless)
H	fin height (m)
H_c	height of flow channel (m)
L	duct length (m)
k	thermal conductivity of air (W/m K)
\dot{m}	mass flow rate (kg/s)
N	number of fins (dimensionless)
Nu	Nusselt number (dimensionless)
P	fin perimeter (m)
Pr	Prandtl number (dimensionless)
$P_{t1}, P_{t2}, P_{d4}, P_{d5}, P_{d6}$	geometric dimension identifying the location of cannellure structure (m), shown in Table 1

\dot{Q}	heat transfer rate (W)
$S_1, S_2, P_{d1}, P_{d2}, P_{d3}$	geometric dimension identifying the location of dimple (m), shown in Table 1
T	temperature (K)
V_{ct}	air velocity in the flow channel (m/s)
V_{front}	frontal velocity (m/s)
\dot{V}	volumetric air flow rate (m ³ /s)
W	width of heat sink (m)
x^+	inverse Graetz number (dimensionless)

Greek symbols

ΔT_m	effective mean temperature difference (K)
ΔP	Total Pressure drop (Pa)
δ	thickness of fin (m)
δ_d	dimple height (m), shown in Table 1
ρ	density of air (kg/m ³)

Subscript

air	air
avg	average
in	inlet
plate	plain fin surface
out	outlet

An alternative way to tailor this problem is to introduce longitudinal vortex generator. The longitudinal vortex generator (LVG) is capable of providing certain heat transfer augmentation without significant rise of pressure drop. Yang et al. [7,8] had systematically examined the applicability of various types of vortex generator, including delta wing, triangular winglet, semi circular, and dimples having loose and dense density. One of their major findings is that fewer number of LVG often outperforms those with more LVG. Moreover, the resultant pressure drop is much lower than those interrupted surfaces. They also show that the augmentations via

vortex generator are relatively effective when the flow is in the developing region whereas they become less effective in the fully developed region. This is especially pronounced when the fin spacing is small or operated at a lower frontal velocity. In summary, surfaces employed with LVG are only marginally improved at low velocity region or small fin spacing, yet the plain fin geometry still outperforms most of the fin patterns at the fully developed region. This is because a close spacing prevented the formation of vortex, and the presence of interrupted surfaces/vortex generator may also suffer from constriction of conduction path.

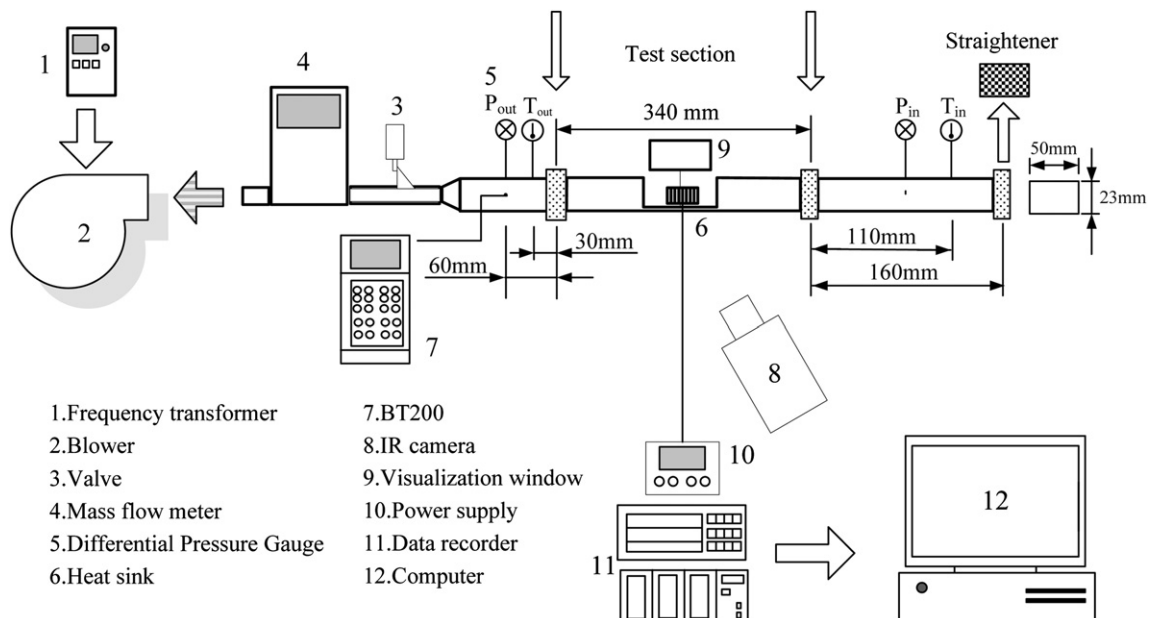


Fig. 1. Experimental set up.

In practice, the electronic cooling applications often use very dense fin for heat dissipation due to space limitation. The dense fin arrangements may lead to early fully developed flow and result in a lower heat transfer performance accordingly. In the situation, it is hard to have an appreciable augmentation. To tackle this problem, the present study proposes a quite unique fin configuration which will be proved to be very effective for applications in highly compact heat sink.

2. Experimental apparatus

The experiment apparatus are setup to measure the heat transfer and the pressure drop characteristics of the heat sinks. Two main parts of the experimental apparatus are described in the following.

2.1. Experimental setup

As seen in Fig. 1, experiments were performed in a channel flow experimental rig which consisted of a closed rectangular channel with a removable test section. The ambient air flow was forced across the test section by a centrifugal fan with an inverter. To avoid and minimize the effect of flow mal-distribution in the experiments, an air straightener–equalizer and a mixer were provided. The inlet and the exit temperatures across the sample were measured by two T-type thermocouple meshes. The inlet measuring

mesh consists of one thermocouple while the outlet mesh contains eight thermocouples. The sensor locations inside the rectangular duct were established following ASHRAE [9] recommendation. These data signals were individually recorded and then averaged. During the isothermal test, the variation of these thermocouples was within 0.2 °C. In addition, all the thermocouples were pre-calibrated by a quartz thermometer having 0.01 °C precision. The accuracies of the calibrated thermocouples are of 0.1 °C. The pressure drop of the test sample was detected by a precision differential pressure transducer, reading to 0.1 Pa. The air flow measuring station was a mass flow meter having 0.2% precision. All the data signals are collected and converted by a data acquisition system (a hybrid recorder). The data acquisition system then transmitted the converted signals through Ethernet interface to the host computer for further operation.

In addition to the heat transfer measurement, a transparent sight glass is installed at the test section to record the temperature along the fin via an Infrared Rays Camera (IR, NEC TH9100PW). The sight glass is made from CVD-ZnSe which is used for production of optical elements for IR range. It has superior transmission in the range of 8–14 μm wavelength. The IR camera is pre-calibrated with a resolution of 0.2 °C. The emissivity of highly polished metal surface is normally poor. Hence for IR operation, the test fin patterns are pre-coated with black paint for precise temperature recording. The black paint is made of synthetic resin, pigment and organic solvents, and the specific emissivity of black paint is 0.94.

Table 1
All tested heat sinks in the present investigation.

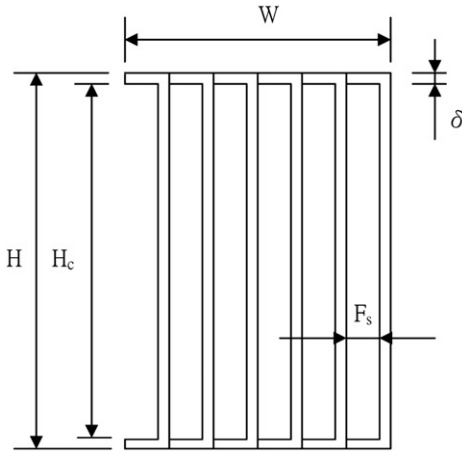
Heat sink	Nomenclature	Side view	Photos of test sample
(a) Plate			
(b) Oblique dimple gap 4-12 fin			
(c) Oblique dimple gap 6-12 fin			
(d) Cannelure fin I			
(e) Cannelure fin II			
(f) Oblique dimple gap 4-12 cannelure fin			
(g) Oblique dimple gap 6-12 cannelure fin I			
(h) Oblique dimple gap 6-12 cannelure fin II			

2.2. Heat sink

A total of eight heat sinks were made and tested, the corresponding fin patterns are (a) plain fin; (b) oblique dimple type (I); (c) oblique dimple type (II); (d) straight cannelure; (e) full oblique cannelure; (f) half oblique cannelure with dimple/cavity type (I); (g) half oblique cannelure with dimple/cavity type (II); (h) full oblique cannelure with dimple/cavity. The difference between type (I) and type (II) is the distance of from the entrance to the first oblique dimple. The distance is 4 mm for type (I) whereas type (II) is 6 mm. The heat sinks are made from copper with a thermal conductivity of 398 W/m K. Detailed locations and photos of the

test heat sink are tabulated in Table 1. The size of dimple and cannelure structure is also shown in Table 2. The corresponding fin pitches is 1.0 mm with a constant fin thickness of 0.2 mm and the height of the heat sinks is 10 mm. A film heater with the same size of base plate is attached to the bottom of heat sink. During the tests, an approximately 3 W power from the electric power supply is provided to the heater. The bakelite board is installed beneath the film heater in order to minimizing the heat loss. However, the actual heat input to the heat sink is determined from the mass flow rate and temperature difference across the heat sink. Normally the heat un-balance (heat loss) amid the film heater and the air side depends on the air velocity. The un-balance is less than 5% for

Table 2
Heat sink dimension (Unit: mm).



L	50		
W	6		
H	10		
F_p	1		
δ	0.2		
	Dimple		cannelure
D	3.05	P_{t1}	0.4
d	2	P_{t2}	0.6
δ_d	0.5	δ_t	0.1
S_d	3.3	A_c	57.5°
P_{d1}	6 (Heat sink c,g,h) or 4 (Heat sink f)	P_{d4}	9.5 (Heat sink e,g,h) or 8 (Heat sink f)
P_{d2}	12	P_{d5}	16.5
P_{d3}	2	P_{d6}	15
δ_d/d	0.25	-	-
F_p/d	0.5	-	-
S_1	1.65	-	-
S_2	3.35		

a frontal velocity of 5 m s^{-1} and is increased to about 30% for a frontal velocity of 10 m s^{-1} . However, the heat loss casts very minor influence on the data reduction for the actual heat transfer rate is determined from the air mass flow rate and the temperature difference across the heat sink. Five temperature sensors were placed below the heat sink to measure the average temperature of the heat sink.

3. Data reduction of the heat sink

The airside performance of the test heat sinks is in terms of pressure drop and heat transfer performance characteristics. For determination of the friction factor of the test samples, an adiabatic test is performed to obtain the total pressure drops. Hence, the measured friction factor can be obtained from the following equation:

$$f = \frac{\Delta P}{4 \left(\frac{L}{D_h}\right) \cdot \left(\frac{\rho V_{ct}^2}{2}\right)} \quad (1)$$

Where L , D_h , and ρ are the duct length, hydraulic diameter and density of air. The hydraulic diameter (D_h) is defined by height of flow channel (H_c) and fin spacing (F_s), and can be obtained from the following equation:

$$D_h = \frac{4A_{ct}}{P} = \frac{4 \times (H_c \times F_s)}{2 \times (H_c + F_s)} \quad (2)$$

Some geometric dimensions can be seen in Table 2. The characteristic velocity is maximum air flow velocity within fin channels:

$$V_{ct} = \frac{\dot{V}}{A_{front} - A_{ft,hs}} \quad (3)$$

Where \dot{V} , A_{front} , and $A_{ft,hs}$ represent the volumetric flow rate, frontal area and the cross sectional fin area of the heat sink. The total heat transfer surface area (A) is the surface in contact with work fluid, and the frontal area of the test section of fin (A_{front}) is:

$$A_{front} = W \times H \quad (4)$$

The cross sectional fin area ($A_{ft,hs}$) can calculate by number of fins (N), fin thickness (δ), width of heat sink (W) and height of flow channel (H_c):

$$A_{ft,hs} = 2 \times \delta \times W + N \times \delta \times H_c \quad (5)$$

The convective heat transfer rate of experimental system can be obtained from the following equation:

$$\dot{Q}_{conv} = \dot{m}Cp_a(T_{air,out} - T_{air,in}) \quad (6)$$

Where \dot{m} , Cp_a , $T_{air,out}$ and $T_{air,in}$ represent mass flow rate, specific heat, average temperature of the inlet test section and the average temperature of the outlet test section.

The effective heat transfer coefficients are evaluated from the ratio of heat transfer rate to the total surface area and temperature difference of wall and air:

$$\bar{h} = \frac{\dot{Q}_{conv}}{A_{plate}(T_w - T_{air,avg})} \quad (7)$$

Where T_w is the average surface temperature and $T_{air,avg}$ is the average temperature of the air at the test section. The heat transfer performance can be of dimensionless Nusselt number and Colburn j factor as

$$Nu = \frac{\bar{h}D_h}{k} \quad (8)$$

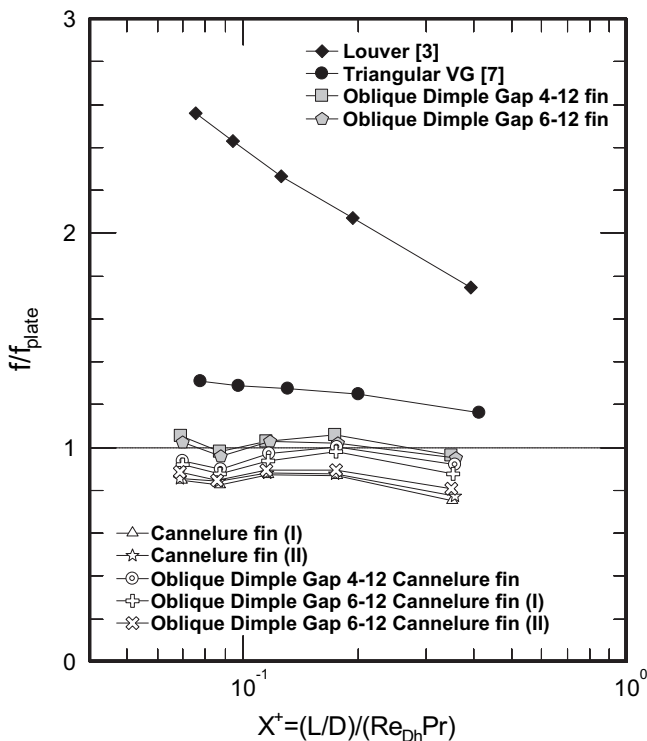


Fig. 2. Inverse Graetz number x^+ vs. f/f_{plain} for the test heat sinks.

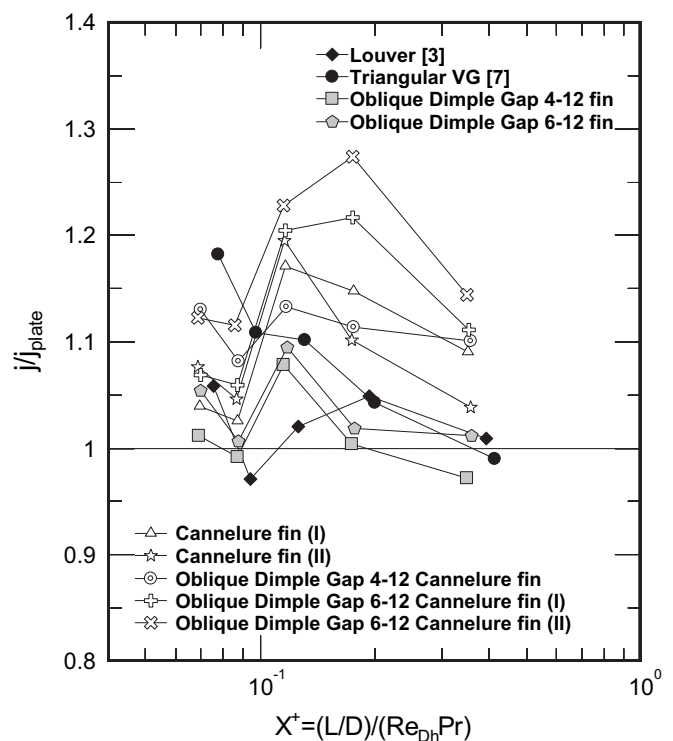


Fig. 3. Inverse Graetz number x^+ vs. j/j_{plain} for the test heat sinks.

$$j = \frac{\bar{h}}{\rho V_{ct} C p_a} P r^{2/3} \quad (9)$$

Uncertainties in the reported experimental values were estimated by the method suggested by Moffat [10]. The highest uncertainties are 2.77% for the heat transfer coefficient and 3.02% for f . The highest uncertainties were associated with lowest Reynolds number.

4. Results and discussion

Normally the effective approach of heat transfer improvement (from $Q = hA\Delta T_m$, Q : total heat dissipated, A : area, h : convective heat transfer coefficient, ΔT_m : effective mean temperature difference) is via increasing heat dissipated area, improving convective heat transfer coefficient, or both. In this study, we have investigated various kinds of improvements characterizing the forgoing augmentations. The easier way is just increasing the surface area by reducing the fin spacing. However, it also accompanies substantial rise of pressure drop, yet smaller fin spacing may result in fully developed flow, leading to a deterioration of heat transfer performance. In this regard, the aim of this study is to propose some certain fin configurations for heat transfer augmentation.

For a further comparison about the influence of developing flow on the heat transfer performance, test results for the proposed fin configurations are plotted in terms of f/f_{plain} and j/j_{plain} vs. the inverse Graetz number as depicted in Figs. 2 and 3. For comparison purpose, prior results for the interrupted surface (Yang et al. [3]) and triangular winglet (Yang et al. [7]) are included. As shown in Figs. 2 and 3, the interrupted fin shows a pronounced frictional penalty with barely no heat transfer augmentation (on the order of

5%), followed by the LVG with significant drop of pressure drop penalty along with some increase of heat transfer performance. Note that the heat transfer augmentation for LVG is comparatively effective at the entrance region but only marginal enhancement in the fully developed region is seen. The reasons for the ineffectiveness of interrupted surface and the marginal increase of LVG at low Reynolds number had been explained in the introduction section.

On the other hand, it is found that the cannelure structure can significantly reduce the pressure drop. In fact, all the fin surfaces with cannelure structure show an appreciable reduction of pressure drop. The pressure drop reduction rises with the effective length of cannelure structure. In fact, the pressure drops for straight or oblique cannelure structure having full length are the smallest among the test heat sinks, and the corresponding reduction in pressure drop can be as large as 20% while the reduction remains almost the same in both developing and fully developed region. Note that normally an inverse Graetz number (x^+) less than 0.1 is regarded as developing and the opposite ($x^+ > 0.1$) is considered as fully developed.

By imposing the dimple/cavity structure to the fin surface will lead to a rise of pressure drop accordingly, yet the pressure drops for the combination of dimple/cavity and cannelure structure are between these two configurations. The fin structure with only dimple/cavity shows a slightly increase of pressure drop as compared to the plain fin surface. Possible explanation of the pressure drop of the cannelure structure will be given after the discussion of the heat transfer part.

The heat transfer improvement relative to the plain fin structure is given in Fig. 3. As depicted in the figure, the heat transfer performance for all the cannelure configurations are higher than that of plain fin surface, yet the superimposed dimple/cavity structure onto the cannelure structure reinforces the heat transfer

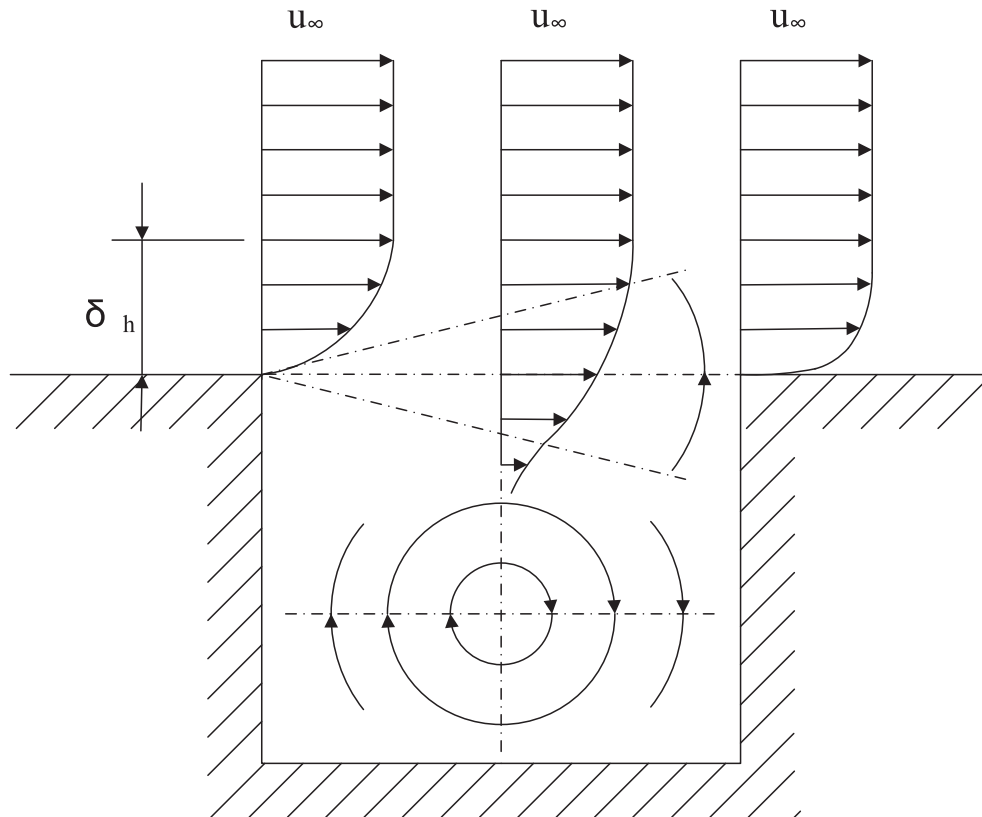


Fig. 4. Schematic of the air flow across an isolated rectangular pit (based on [14]).

augmentations. It is interesting to know that the cannellure structure is especially effective in fully developed region where other enhancements like interrupted or vortex generator are quite ineffective. A possible mechanism for the appreciable heat transfer enhancement for the cannellure structure in fully developed flow region is due to the near wall vortices being generated. For a further elaboration of this phenomenon, one can see a schematic

illustrated in Fig. 4. For flow in fully developed region, the approaching flow distribution is parabolic on the left hand side of the schematic. As the air flows above the cannellure structure, the velocity profile is strength subject to no slip condition at the bottom of the cannellure structure, yet a vortical motion emerges from this velocity distribution. As the air approaches the end of cannellure structure, it separates into two streams (above and below the

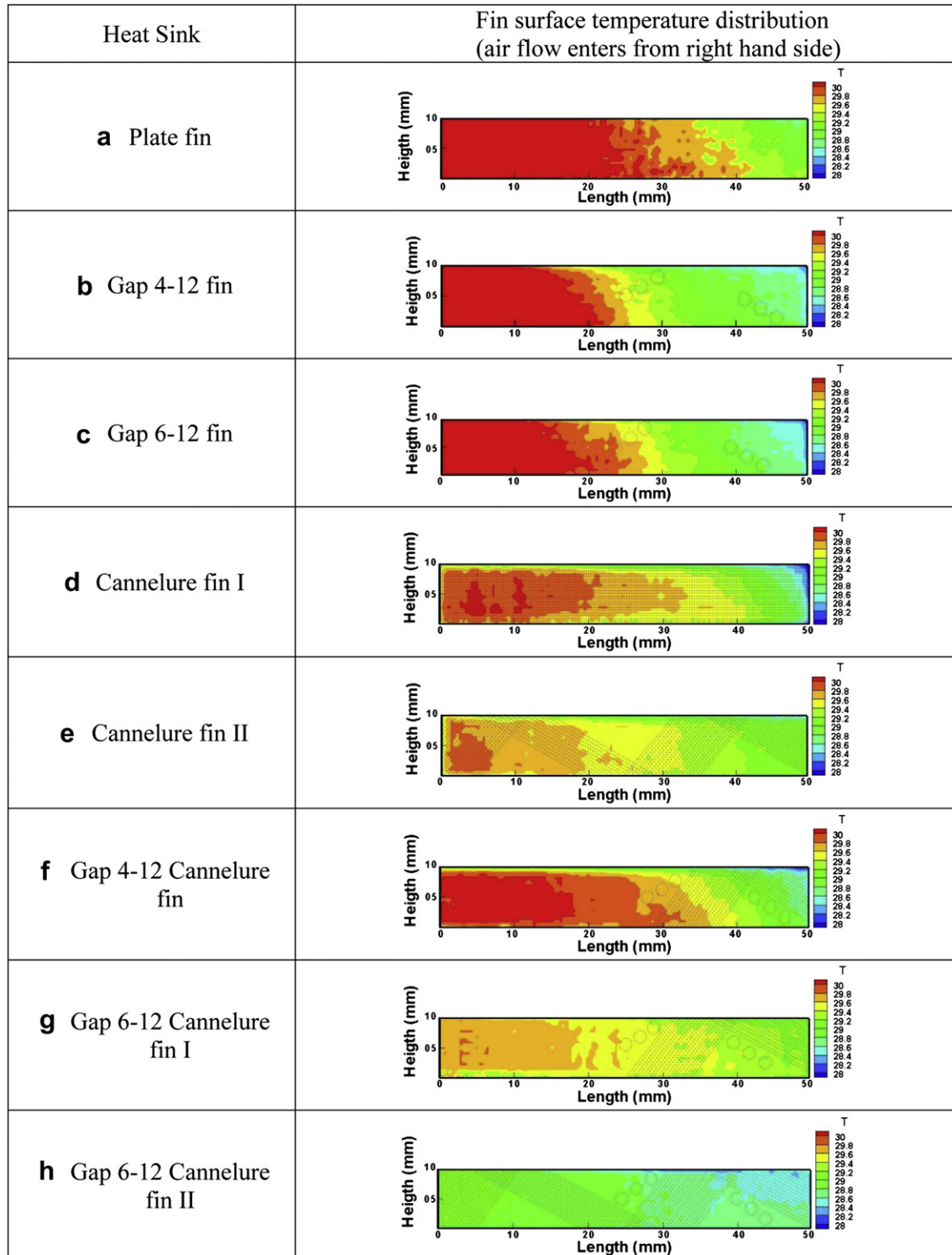


Fig. 5. Fin surface temperature distribution by IR image for an inlet frontal velocity of 5 m s⁻¹.

cannelure depth), the stream above the cannelure is with a higher velocity profile nears the surface as compared to fully developed profile in front of the cannelure. In the meantime, the stream below the cannelure structure encountered the end of cannelure and rise to become an upwash stream similar to the cavity structure [11]. The upwash flow along with the flow distribution passing the cannelure form a near wall vortical motion, and this will lead to a rise in heat transfer. In summary, the resultant near wall vortical structure is similar to a suction/blowing flow through which appreciable heat transfer enhancement can be achieved without pressure drop penalty (Kasagi et al. [12]). Kasagi et al. [12] conducted extensive numerical experiments using a local suction/blowing as an input, and had clearly identified the control of this near wall structure can significant increase the heat transfer performance with a negligible increase or even decrease of the pressure drop. Choi et al. [13] had proposed the so-called opposition control based on the knowledge of near-wall coherent turbulent structures. They demonstrated in their direct numerical simulation that approximately 25% drag reduction can be attained by applying local blowing/suction so as to oppose the wall-normal velocity fluctuation near the wall. Afans'yev et al. [14] also shows a 30% increase of heat transfer performance with a negligible increase of pressure drop for flow across a pit/groove along a smooth wall.

The superimposed dimple/cavity structure will induce further transverse motion that may strengthen the near wall vortical structure, leading to a further enhancement. Note that the near wall vortical structure is especially effective in fully developed region. This is because the generated near wall vortical structure can effectively exchange the fluid amid wall surface and bulk region.

The foregoing results can be further verified from the local temperature distribution of the fin surface using the IR image recorder as shown in Fig. 5 for an inlet frontal velocity of 5 m/s. In Fig. 5(a), the fin surface temperature distribution for plain fin surface remains comparatively low and become almost constant after 20 mm from the inlet. The distance then moves to approximately 30 mm by imposing the dimple/cavity structure in Fig. 5(b). With introducing the cannelure structure, the higher temperature region is moved further toward the end of heat sink (Fig. 5(e)), and the higher temperature almost disappears when dimple/cavity structure is introduced to the cannelure structure (Fig. 5(h)). The foregoing IR images indirectly confirm the possible augmentation mechanism of the cannelure configuration.

5. Conclusions

The present study proposed a novel cannelure fin structure applicable to air-cooled heat sink under cross flow condition. A total of eight heat sinks were made and tested, the corresponding fin patterns are (a) plain fin; (b) oblique dimple type (I); (c) oblique dimple type (II); (d) straight cannelure; (e) full oblique cannelure; (f) half oblique cannelure with dimple/cavity type (I); (g) half

oblique cannelure with dimple/cavity type (II); (h) full oblique cannelure with dimple/cavity. The test heat sinks are with a fin spacing of 0.8 mm. Test results indicate that the proposed cannelure fin configuration along with the dimple/cavity structure can attain an approximately 25% increase of heat transfer performance, and accompanies a friction reduction of about 20%. Moreover, converse to those interrupted fin or common vortex generator, it is found that the proposed fin structure still offers significant augmentation in fully developed region. The possible mechanism for appreciable increase of heat transfer without suffering the pressure drop penalty is attributed to the local suction/blowing flow and the near wall vortical motion caused by the cannelure structure. The observed IR image had indirectly confirmed the likely mechanism.

Acknowledgements

The author is indebted to the financial support (99-2622-E-009-016-CC2) from the National Science Council, Taiwan and the Bureau of Energy, Ministry of Economic Affairs, Taiwan.

References

- [1] S. Trutassanawin, E.A. Groll, S.V. Garimella, L. Cremaschi, Experimental investigation of a miniature-scale refrigeration system for electronics cooling, *IEEE T. Compon. Pack. T.* 29 (2006) 678–687.
- [2] M. Saini, R.L. Webb, Heat rejection limits of air cooled plane fin heat sinks for computer cooling, *IEEE T. Compon. Pack. T.* 26 (2003) 71–79.
- [3] K.S. Yang, C.M. Chiang, Y.T. Lin, K.H. Chien, C.C. Wang, On the heat transfer characteristics of heat sinks: influence of fin spacing at low Reynolds number region, *Int. J. Heat Mass Transfer* 50 (2007) 2667–2674.
- [4] R.L. Webb, P. Trauger, Flow structure in the louvered fin heat exchanger geometry, *Exp. Therm. Fluid Sci.* 4 (1991) 205–217.
- [5] C.J. Davenport, Correlations for heat transfer and flow friction characteristics of louvered fin, *AIChE Symp. Ser.* 79 (1983) 19–27.
- [6] A. Achaichia, T.A. Cowell, Heat transfer and pressure drop characteristics of flat tube and louvered plate fin surface, *Exp. Therm. Fluid Sci.* 1 (1988) 147–157.
- [7] K.S. Yang, J.H. Jhong, Y.T. Lin, K.H. Chien, C.C. Wang, On the heat transfer characteristics of heat sinks: with and without vortex generators, *IEEE T. Compon. Pack. T.* 33 (2010) 391–397.
- [8] K.S. Yang, S.L. Li, I.Y. Chen, K.H. Chien, C.C. Wang, Analysis of air cooling thermal module using various enhancements at low Reynolds number region, *Int. J. Heat Mass Transfer*, Accepted.
- [9] ASHRAE Handbook Fundamental SI-Edition. American Society of Heating, Refrigerating and Air-conditioning Engineers, Inc., Atlanta, 1993, pp. 13.14–13.15.
- [10] R.J. Moffat, Describing the uncertainties in experimental results, *Exp. Therm. Fluid Sci.* 1 (1988) 3–17.
- [11] H.L. Haugen, A.M. Dhanak, Momentum transfer in turbulent separated flow past a rectangular cavity, *J. Appl. Mech. Trans. ASME* (1966) 464–641.
- [12] N. Kasagi, Y. Hasegawa, K. Fukagata, K. Iwamoto, Control of turbulent transport: less friction and more heat transfer, in: *Proceedings of the 14th International Heat Transfer Conference, IHTC-14*, August 8–13 2010, Washington D.C., USA, IHTC14-23344.
- [13] H. Choi, P. Moin, J. Kim, Active turbulence control for drag reduction in wall-bounded flows, *J. Fluid Mech.* 262 (1994) 75–110.
- [14] V.N. Afans'yev, V.Y. Veselkin, A.I. Leontiev, A.P. Skibin, P. Chudnovskiy, Thermohydraulics of flow over isolated depressions (pits, grooves) in a smooth wall, *Heat Transfer Res.* 25 (1993) 22–56.